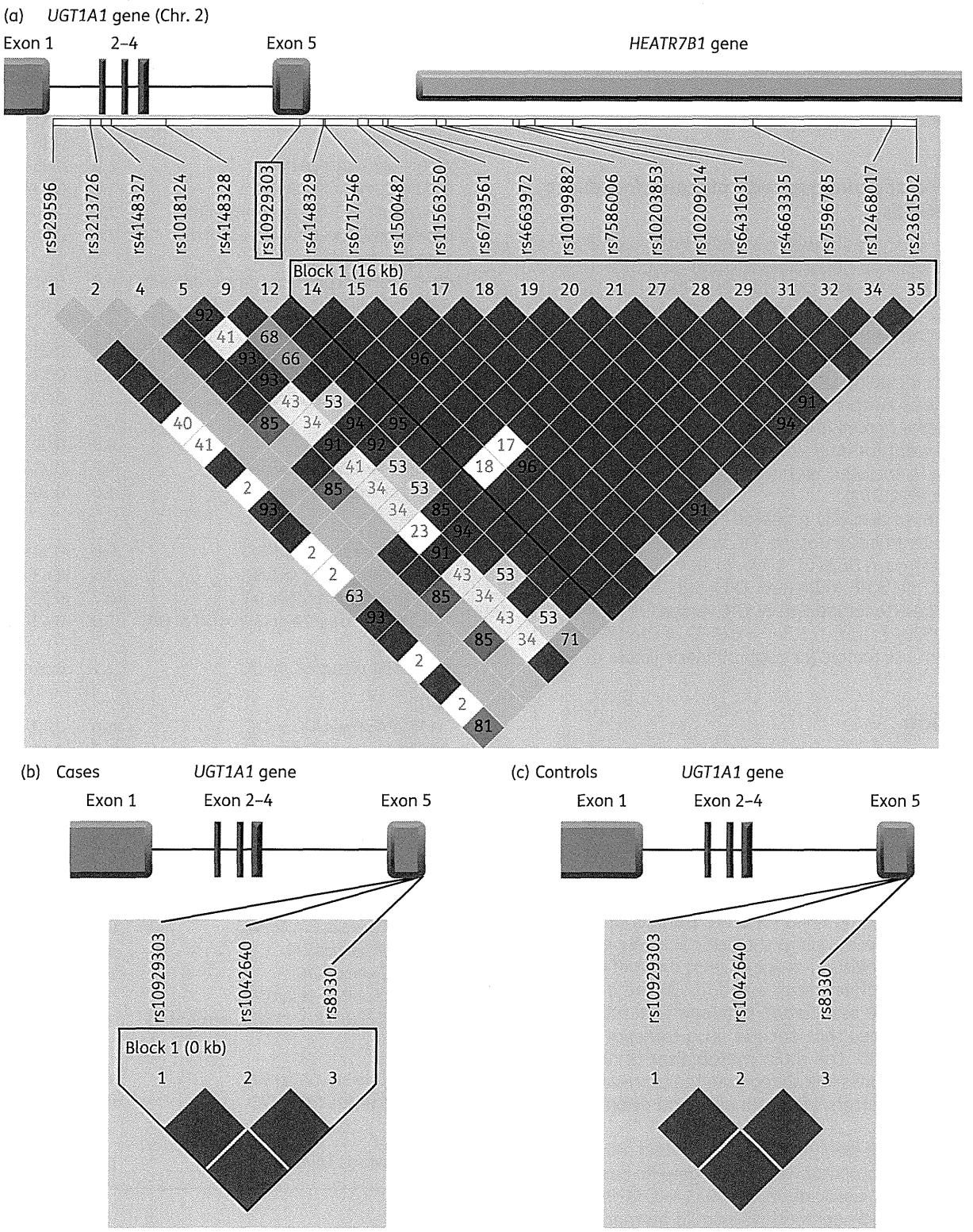

Figure 1. Pairwise linkage disequilibrium analysis of *UGT1A1* and surrounding SNPs. (a) Pairwise linkage disequilibrium analysis of *UGT1A1* and surrounding SNPs using HapMap Japanese samples. SNP c.211 (rs10929303) of the UGT1A-3′-UTR is in tight linkage disequilibrium with the gene next to *UGT1A1* (*HEATR7B1*). Two SNPs at 339 (rs1042640) and 440 (rs8330) of the UGT1A-3′-UTR are not shown in (a), but they are located close to c.211, as shown in (b) and (c). Pairwise linkage disequilibrium analysis of the three risk SNPs in the UGT1A-3′-UTR in (b) 31 cases (patients with atazanavir-induced nephrolithiasis) and (c) 47 controls. The difference between (b) and (c) suggests that the number of risk haplotypes is greater in case patients than in control patients. Estimates of *D′* for SNPs are shown as numbers in the Argyle box. Dark red shading indicates strong linkage disequilibrium (*D′* >0.9). Light blue shading indicates high *D*' values (>0.99) with low statistical significance [LOD (log of the odds) <2].

shows the results of pairwise linkage disequilibrium analysis of *UGT1A1* and SNPs around them derived from HapMap data for the Japanese. On the other hand, there was no difference in the distribution of 16 other SNPs in *ABCB1*, *NR1I2*, *SLCO1B1* and *CYP3A5* between cases and controls. The distribution of UGT1A1*28 was also not different.

Association of genotypes with atazanavir-induced nephrolithiasis

Univariate analysis showed a significant association between atazanavir-induced nephrolithiasis and genotype T/C versus C/C at c.211 (OR=3.8; 95% CI, 1.22–11.6; P=0.022), genotype G/C versus C/C at position 339 (OR=5.9; 95% CI, 1.68–20.9; P=0.006) and genotype G/G or G/C versus C/C at 440 (OR=5.9; 95% CI, 1.68–20.9; P=0.006) of the UGT1A-3′-UTR (Table 3). No other SNPs, including UGT1A1*28, showed any association with nephrolithiasis. Furthermore, basic demographics and established risk factors for nephrolithiasis were not associated with nephrolithiasis, except for infection with hepatitis C virus, which was marginally associated with nephrolithiasis (OR=8.8; 95% CI, 0.98–79.9; P=0.052).

Multivariate analysis adjusted for sex, age and hepatitis C infection identified genotype T/C versus C/C at position c.211 (adjusted OR=3.7; 95% CI, 1.13–11.9; P=0.030), genotype G/C versus C/C at 339 (adjusted OR=5.8; 95% CI, 1.56–21.3; P=0.009) and genotype G/G or G/C versus C/C at 440 (adjusted OR=5.8; 95% CI, 1.56–21.3; P=0.009) of the UGT1A-3′-UTR as independent risk factors for nephrolithiasis (Table 4).

Table 3. Univariate analysis to estimate the association of various factors with atazanavir-induced nephrolithiasis

	OR	95% CI	*P* value
Male	1.7	0.31–9.51	0.53
Age per year	1.0	0.93–1.03	0.39
Weight per 1 kg increment	1.0	0.95–1.03	0.60
BMI per 1 kg/m^2 increment	1.0	0.83–1.11	0.58
CD4 count per 1 cell/mm^3 increment	1.0	1.00–1.00	0.63
Baseline eGFR per 1 mL/min/1.73 m^2 decrement	1.0	0.98–1.03	0.80
HIV-1 viral load per 1 $\log_{10}$/mL increment	0.9	0.62–1.34	0.64
Hepatitis C infection	8.8	0.98–79.9	0.052
Hepatitis B infection	1.5	0.09–25.5	0.77
Treatment naive	0.7	0.25–1.66	0.37
History of nephrolithiasis	3.3	0.57–19.4	0.18
Uric acid per 1 mg/dL increment	1.2	0.93–1.56	0.16
Hypertension	0.7	0.17–3.17	0.68
Diabetes mellitus	0.8	0.07–8.64	0.82
Co-administration of tenofovir	0.7	0.27–1.92	0.51
History of indinavir use	1.6	0.30–8.34	0.60
ABCB1			
193 A/A versus A/G or G/G	0.8	0.32–1.97	0.61
365 T/T versus T/C or C/C	2.5	0.63–10.0	0.19
1236 C/C versus C/T or T/T	0.7	0.22–2.33	0.57
2677 T/T versus T/A or G/G or G/T or G/A or A/A	1.6	0.43–6.12	0.48
3435 T/T versus T/C or C/C	2.1	0.51–8.40	0.31
NR1I2			
131 A/A versus A/C or C/C	1.0	0.40–2.58	0.97
370 G/G versus G/A or A/A	0.7	0.25–1.84	0.44
522 C/C versus C/T or T/T	0.7	0.27–2.04	0.56
1195 C/C versus C/A or A/A	0.7	0.30–2.27	0.70
1232 C/C versus C/T or T/T	0.7	0.25–1.84	0.44
44477 C/C versus C/T or T/T	1.1	0.42–2.67	0.89
63396 C/C versus C/T or T/T	2.2	0.45–10.5	0.33
UGT1A1			
211 G/G versus G/A or A/A	0.9	0.35–2.29	0.82
c.211 T/C versus C/C	3.8	1.22–11.6	0.022
339 G/C versus C/C	5.9	1.68–20.9	0.006
440 G/G or G/C versus C/C	5.9	1.68–20.9	0.006
UGT1A1 *28/*28 or *28/*1 versus *1/*1	2.2	0.45–10.5	0.33
SLCO1B1			
388 G/G versus G/A or A/A	1.6	0.30–8.34	0.60
521 T/T versus T/C or C/C	0.9	0.36–2.43	0.90
CYP3A5			
14 T/T versus T/C or C/C	0.9	0.38–2.33	0.89

Discussion

To our knowledge, this is the first study that has elucidated the association between genetic polymorphisms in the genes encoding proteins that affect atazanavir exposure and atazanavir-induced nephrolithiasis. The results demonstrated that Japanese HIV-1-infected patients who developed atazanavir-induced nephrolithiasis were ~5-fold more likely to have variants in the UGT1A-3′-UTR, compared with those without nephrolithiasis, who were well-matched for other traditional risk factors for nephrolithiasis. These findings suggest a link between genetic factors and nephrolithiasis, a major adverse event of atazanavir that can significantly affect renal function. On the other hand, the results showed no association between variants in *ABCB1* and *SLCO1B1*, the genes that encode drug transporter protein for atazanavir, *CYP3A5*, the main metabolizer of atazanavir, and *NR1I2*, which encodes PXR to regulate the expression of metabolizers and transporters of atazanavir, and atazanavir-induced nephrolithiasis.

This study enrolled only Japanese patients in order to examine a population with comparatively similar genetic backgrounds. It is possible that the association of UGT1A-3′-UTR variants with atazanavir-induced nephrolithiasis could be more significant in people of African or European origin than Japanese or East Asians, considering that the allele frequencies of these variants are higher in these populations according to the HapMap data [e.g. minor allele frequency at position 440 (rs8330): Africans 50%, Europeans 23.3%, Japanese 15.9%, Chinese 15.6%] (www.hapmap.org). Similar studies are needed in these populations to confirm that the association between UGT1A-3′-UTR variants and atazanavir-induced nephrolithiasis is reproducible.

The mechanism by which SNPs in the UGT1A-3′-UTR are associated with the development of nephrolithiasis in patients on an atazanavir-containing regimen is unknown. However, Court

Table 4. Multivariate analysis to estimate the association of SNPs of the UGT1A-3′-UTR with atazanavir-induced nephrolithiasis

UGT1A-3′-UTR	Adjusted OR	95% CI	*P* value
Genotype T/C versus C/C at position c.211	3.7	1.13–11.9	0.030
Genotype G/C versus C/C at position 339	5.8	1.56–21.3	0.009
Genotype G/G or G/C versus C/C at position 440	5.8	1.56–21.3	0.009

Each SNP was tested in the model separately.
Each variable was adjusted for sex, age and hepatitis C infection.

et al.[32] reported that these SNPs are associated with inter-individual variability in acetaminophen (paracetamol) glucuronidation in the human liver, and provide protection against acute liver failure by acetaminophen overdose, probably through more extensive detoxification of acetaminophen via glucuronidation. Because the biotransformation pathways of atazanavir or its metabolites also include glucuronidation,[12] the UGT1A-3′-UTR variants could alter atazanavir metabolism and pharmacokinetics, resulting in increased atazanavir concentration in the blood and increased excretion in urine, facilitating nephrolithiasis formation. Unfortunately, serum and urine concentrations of atazanavir were not measured in the present study. It is also notable that the *UGT1* subfamily has a unique gene structure; the *UGT1* gene has 13 exon 1s from *UGT1A1* to *UGT1A13P*, and exons 2–5, which are common in all mRNAs expressed from the gene.[36] The UGT1A-3′-UTR is located in exon 5, which is commonly present in the UGT1 subfamily (Figure 1), and thus the variants in the UGT1A-3′-UTR might influence not only UGT1A1 but also other UGT1 isoforms that take part in glucuronidation of various substrates,[36] and they might affect atazanavir metabolism and pharmacokinetics as well. Figure 1 also shows that the identified SNPs in the UGT1 3′-UTR are in tight linkage disequilibrium with the gene next to them (*HEATR7B1*), suggesting that the latter could also affect atazanavir metabolism/transportation. To our knowledge, however, there is no information on the role of *HEATR7B1* in drug metabolism/transportation, and the above conjecture remains to be investigated.

In this study, the median serum total bilirubin level in the case patients was higher than that in the control group. Rockwood *et al.*[8] reported a close relationship between hyperbilirubinaemia and the development of atazanavir-induced renal stones. However, no such relationship was found in our previous cohort study.[6] In two pharmacokinetics studies, Rodríguez-Nóvoa *et al.*[20,29] reported that serum bilirubin level correlated with plasma atazanavir concentration, and one can speculate that high bilirubin levels might reflect higher atazanavir concentrations, which result in precipitation of atazanavir in urine and renal stone formation. However, these results are still preliminary and further studies are needed to determine the true relationship between serum bilirubin level and atazanavir-related nephrolithiasis.

Several limitations of this study need to be acknowledged. First, and importantly, although this study identified association between the UGT1A-3′-UTR variants and atazanavir-induced nephrolithiasis, the number of enrolled patients was small in this case–control study; the results need to be interpreted with caution. The results could provide the basis for an exploratory hypothesis and further larger studies are needed to confirm such an association. Second, not all polymorphisms in genes of the targeted proteins were examined. Thus, we might have missed other important SNPs associated with or affecting the metabolism or transportation of atazanavir. There might be other, unknown proteins that take part in the metabolism or transportation of atazanavir that also contribute to susceptibility to atazanavir-induced nephrolithiasis. Third, because renal stone formation occurs as a composite of various factors and the components of nephrolithiasis were not analysed in the study, it is difficult to exclude the effects of classic risk factors for renal stone formation, apart from the genetic factors identified in the present study. However, the two study samples were well matched in terms of risk factors, such as BMI, serum uric acid and history of indinavir use.[4,5,24–26] Furthermore, the susceptibility to nephrolithiasis in patients on an atazanavir/ritonavir-containing regimen is well established; the incidence of nephrolithiasis is 10- to 20-fold higher in patients on atazanavir/ritonavir-containing ART than in patients on other protease inhibitor-containing ART regimens.[6,7] Fourth, because functional data are not yet available, clinical or biochemical studies to confirm the results obtained here are certainly needed. We did not measure atazanavir concentration in blood or urine.

In conclusion, in a setting where other predisposing factors for nephrolithiasis were well matched, the present study demonstrates that the Japanese HIV-1-infected patients who developed atazanavir-induced nephrolithiasis were ~5-fold more likely to have variants in the UGT1A-3′-UTR compared with those without nephrolithiasis. Further studies are warranted to confirm this association and to elucidate how these SNPs might influence the metabolism and excretion of atazanavir and the formation of nephrolithiasis.

Acknowledgements

We thank Mikiko Ogata, Michiyo Ishisaka and Misao Takano for invaluable contributions to the study. We also thank Akiko Nakano, the study coordinator, and all the other staff at the AIDS Clinical Center for their help in the completion of this study.

Funding

This work was supported by a Grant-in Aid for AIDS research from the Japanese Ministry of Health, Labour, and Welfare (H23-AIDS-001) and the Grant for National Center for Global Health and Medicine (25-106).

Transparency declarations

S. O. has received honoraria and research grants from MSD K.K., Abbott Japan, Co., Janssen Pharmaceutical K.K., Pfizer, Co. and Roche Diagnostics K.K., and has received honoraria from Astellas Pharmaceutical K.K., Bristol-Myers K.K., Daiichisankyo, Co., Dainippon Sumitomo Pharma, Co., GlaxoSmithKline, K.K., Taisho Toyama Pharmaceutical, Co., Torii Pharmaceutical, Co. and ViiV Healthcare. H. G. has received honoraria from MSD K.K., Abbott Japan, Co., Janssen Pharmaceutical K.K., Torii

Pharmaceutical, Co., Roche Diagnostics K.K. and ViiV Healthcare, Co. All other authors: none to declare.

References

1 Panel on Antiretroviral Guidelines for Adults and Adolescents. *Guidelines for the Use of Antiretroviral Agents in HIV-1-Infected Adults and Adolescents.* American Department of Health and Human Services. http://www.aidsinfo.nih.gov/ContentFiles/AdultandAdolescentGL.pdf.

2 Chang HR, Pella PM. Atazanavir urolithiasis. *N Engl J Med* 2006; **355**: 2158–9.

3 Anderson PL, Lichtenstein KA, Gerig N *et al.* Atazanavir-containing renal calculi in an HIV-infected patient. *AIDS* 2007; **21**: 1060–2.

4 Chan-Tack KM, Truffa MM, Struble KA *et al.* Atazanavir-associated nephrolithiasis: cases from the US Food and Drug Administration's Adverse Event Reporting System. *AIDS* 2007; **21**: 1215–8.

5 Couzigou C, Daudon M, Meynard JL *et al.* Urolithiasis in HIV-positive patients treated with atazanavir. *Clin Infect Dis* 2007; **45**: e105–8.

6 Hamada Y, Nishijima T, Watanabe K *et al.* High incidence of renal stones among HIV-infected patients on ritonavir-boosted atazanavir than in those receiving other protease inhibitor-containing antiretroviral therapy. *Clin Infect Dis* 2012; **55**: 1262–9.

7 Nishijima T, Hamada Y, Watanabe K *et al.* Ritonavir-boosted darunavir is rarely associated with nephrolithiasis compared with ritonavir-boosted atazanavir in HIV-infected patients. *PLoS One* 2013; **8**: e77268.

8 Rockwood N, Mandalia S, Bower M *et al.* Ritonavir-boosted atazanavir exposure is associated with an increased rate of renal stones compared with efavirenz, ritonavir-boosted lopinavir and ritonavir-boosted darunavir. *AIDS* 2011; **25**: 1671–3.

9 Rule AD, Bergstralh EJ, Melton LJ 3rd *et al.* Kidney stones and the risk for chronic kidney disease. *Clin J Am Soc Nephrol* 2009; **4**: 804–11.

10 Jungers P, Joly D, Barbey F *et al.* ESRD caused by nephrolithiasis: prevalence, mechanisms, and prevention. *Am J Kidney Dis* 2004; **44**: 799–805.

11 Alexander RT, Hemmelgarn BR, Wiebe N *et al.* Kidney stones and kidney function loss: a cohort study. *BMJ* 2012; **345**: e5287.

12 Reyataz (atazanavir sulfate): full prescription information (package insert). Princeton, NJ: Bristol-Myers Squibb, 2012.

13 Crixivan (indinavir sulfate): full prescription information (package insert). Whitehouse Station, NJ: Merck & Co., Inc., 2012.

14 Wempe MF, Anderson PL. Atazanavir metabolism according to CYP3A5 status: an in vitro-in vivo assessment. *Drug Metab Dispos* 2011; **39**: 522–7.

15 Kile DA, MaWhinney S, Aquilante CL *et al.* A population pharmacokinetic-pharmacogenetic analysis of atazanavir. *AIDS Res Hum Retroviruses* 2012; **28**: 1227–34.

16 Lehmann JM, McKee DD, Watson MA *et al.* The human orphan nuclear receptor PXR is activated by compounds that regulate CYP3A4 gene expression and cause drug interactions. *J Clin Invest* 1998; **102**: 1016–23.

17 Geick A, Eichelbaum M, Burk O. Nuclear receptor response elements mediate induction of intestinal MDR1 by rifampin. *J Biol Chem* 2001; **276**: 14581–7.

18 Siccardi M, D'Avolio A, Baietto L *et al.* Association of a single-nucleotide polymorphism in the pregnane X receptor (PXR 63396C→T) with reduced concentrations of unboosted atazanavir. *Clin Infect Dis* 2008; **47**: 1222–5.

19 Kis O, Zastre JA, Hoque MT *et al.* Role of drug efflux and uptake transporters in atazanavir intestinal permeability and drug-drug interactions. *Pharm Res* 2013; **30**: 1050–64.

20 Rodríguez-Nóvoa S, Barreiro P, Rendón A *et al.* Plasma levels of atazanavir and the risk of hyperbilirubinemia are predicted by the 3435C→T polymorphism at the multidrug resistance gene 1. *Clin Infect Dis* 2006; **42**: 291–5.

21 Tozzi V. Pharmacogenetics of antiretrovirals. *Antiviral Res* 2010; **85**: 190–200.

22 Ma Q, Brazeau D, Zingman BS *et al.* Multidrug resistance 1 polymorphisms and trough concentrations of atazanavir and lopinavir in patients with HIV. *Pharmacogenomics* 2007; **8**: 227–35.

23 Hartkoorn RC, Kwan WS, Shallcross V *et al.* HIV protease inhibitors are substrates for OATP1A2, OATP1B1 and OATP1B3 and lopinavir plasma concentrations are influenced by SLCO1B1 polymorphisms. *Pharmacogenet Genomics* 2010; **20**: 112–20.

24 Parmar MS. Kidney stones. *BMJ* 2004; **328**: 1420–4.

25 Chan-Tack KM, Edozien A. Ritonavir-boosted atazanavir may be efficacious in HIV-infected patients concurrently receiving omeprazole. *Clin Infect Dis* 2006; **42**: 1344.

26 Ando R, Nagaya T, Suzuki S *et al.* Kidney stone formation is positively associated with conventional risk factors for coronary heart disease in Japanese men. *J Urol* 2013; **189**: 1340–6.

27 Taylor EN, Stampfer MJ, Curhan GC. Diabetes mellitus and the risk of nephrolithiasis. *Kidney Int* 2005; **68**: 1230–5.

28 Levey AS, Coresh J, Greene T *et al.* Using standardized serum creatinine values in the Modification of Diet in Renal Disease study equation for estimating glomerular filtration rate. *Ann Intern Med* 2006; **145**: 247–54.

29 Rodríguez-Nóvoa S, Martín-Carbonero L, Barreiro P *et al.* Genetic factors influencing atazanavir plasma concentrations and the risk of severe hyperbilirubinemia. *AIDS* 2007; **21**: 41–6.

30 Park WB, Choe PG, Song KH *et al.* Genetic factors influencing severe atazanavir-associated hyperbilirubinemia in a population with low UDP-glucuronosyltransferase 1A1*28 allele frequency. *Clin Infect Dis* 2010; **51**: 101–6.

31 Takeuchi K, Kobayashi Y, Tamaki S *et al.* Genetic polymorphisms of bilirubin uridine diphosphate-glucuronosyltransferase gene in Japanese patients with Crigler-Najjar syndrome or Gilbert's syndrome as well as in healthy Japanese subjects. *J Gastroenterol Hepatol* 2004; **19**: 1023–8.

32 Court MH, Freytsis M, Wang X *et al.* The UDP-glucuronosyltransferase (UGT) 1A polymorphism c.2042C>G (rs8330) is associated with increased human liver acetaminophen glucuronidation, increased UGT1A exon 5a/5b splice variant mRNA ratio, and decreased risk of unintentional acetaminophen-induced acute liver failure. *J Pharmacol Exp Ther* 2013; **345**: 297–307.

33 Hirakawa M, Tanaka T, Hashimoto Y *et al.* JSNP: a database of common gene variations in the Japanese population. *Nucleic Acids Res* 2002; **30**: 158–62.

34 Rotger M, Taffe P, Bleiber G *et al.* Gilbert syndrome and the development of antiretroviral therapy-associated hyperbilirubinemia. *J Infect Dis* 2005; **192**: 1381–6.

35 Beutler E, Gelbart T, Demina A. Racial variability in the UDP-glucuronosyltransferase 1 (UGT1A1) promoter: a balanced polymorphism for regulation of bilirubin metabolism? *Proc Natl Acad Sci USA* 1998; **95**: 8170–4.

36 Maruo Y, Iwai M, Mori A *et al.* Polymorphism of UDP-glucuronosyltransferase and drug metabolism. *Curr Drug Metab* 2005; **6**: 91–9.

Degeneration, Regeneration, and Cicatrization after Fat Grafting: Dynamic Total Tissue Remodeling during the First 3 Months

Harunosuke Kato, M.D.
Kazuhide Mineda, M.D.
Hitomi Eto, M.D.
Kentaro Doi, M.D.
Shinichiro Kuno, M.D.
Kahori Kinoshita, M.D.
Koji Kanayama, M.D.
Kotaro Yoshimura, M.D.

Tokyo, Japan

Background: Fat grafting is promising, but clinical outcomes are not always predictable. The mechanisms of tissue revascularization/regeneration, and tissue necrosis and subsequent absorption/fibrosis of the graft, are poorly understood.

Methods: An autologous inguinal fat pad was transplanted under the scalp of mice, and detailed cellular events during the first 3 months were investigated with immunohistochemistry.

Results: Except for the most superficial surviving zone, death of all adipocytes was confirmed at 1 week. Perilipin-positive small new adipocytes appeared at 1 week and peaked in number at 4 weeks in the regenerating zone (the second zone). In the most central necrotizing zone, adipogenesis did not occur and many inflammatory cells were observed after 2 weeks. $CD34^+/Ki67^+$ proliferating adipose stem/progenitor cells were seen at 1 to 4 weeks, but the majority of proliferating cells were $MAC2^+$ monocytes/macrophages. Although $CD206^-$ M1 macrophages surrounded oil droplets for phagocytosis, $CD206^+$ M2 macrophages appeared in areas where adipocyte replacement failed and formed multiple layers for cicatrization of oil drop spaces. Adipogenesis was complete by 12 weeks, but stabilization of nonregenerated areas was still ongoing at that time. Lipid droplets derived from dead adipocytes were absorbed slowly and thus aided adipose remodeling by maintaining the space until adipocyte regeneration.

Conclusions: Dynamic remodeling after fat grafting was confirmed. Adipocyte fate differed, depending on the microenvironment: intact survival, replacement with a new adipocyte, or replacement with cicatrization/oil cyst. This detailed understanding will help refine surgical grafting procedures and postoperative evaluation. (*Plast. Reconstr. Surg.* 133: 303e, 2014.)

Adipose tissue has been widely used as an injectable substance and has been recently reevaluated as a tool not only for augmenting tissue volume (volumization) but also for enhancing tissue potential (revitalization) and modulating immunoreaction (harmonization). Fat grafting has several potential drawbacks, including clinical unpredictability, and thus efforts have focused on seeking ways to achieve improved and more consistent final retention.[1–4] The variability of clinical results originates partly from unique characteristics of adipose tissue; therefore, further research is required to explore the underlying cellular and molecular mechanisms in the healing and remodeling process after fat grafting. It is important to understand not only how the graft is retained, but also how long-term tissue atrophy, oil cyst formation, and progressive calcification occur.

A variety of cell types are present in subcutaneous adipose tissue,[5] and adipocytes account for only 20 percent or less of the total number of cells.[6] We previously reported cellular events during various types of adipose tissue remodeling, such as those seen after surgically induced ischemia,[7] ischemia-reperfusion injury,[8] and fat grafting.[9] In those studies, adipose stem/progenitor/

From the Department of Plastic Surgery, University of Tokyo, School of Medicine.
Received for publication August 7, 2013; accepted September 17, 2013.

DOI: 10.1097/PRS.0000000000000066

Disclosure: *The authors have no financial interest to declare in relation to the content of this article.*

stromal cells were demonstrated to play pivotal roles in adipose tissue repair and regeneration, whereas inflammatory cells, such as infiltrated macrophages, contributed to removing degenerated components. A series of primary and subsequent signals, including hypoxia and cytokines, appear to regulate the complex events during adipose tissue remodeling.[10–14]

We recently presented convincing evidence that most adipocytes (except for those located superficially) die as early as day 1 after fat grafting, and the subsequent regeneration process starts as early as day 5.[9] Adipose stem/progenitor/stromal cells can stay alive for up to 3 days, even under stressful conditions, such as severe hypoxia. Immunohistologic staining for perilipin[15] was the primary technology used to distinguish living from dead adipocytes and verify dynamic adipocyte replacement in the grafted fat tissue.

The present study was designed to clarify the detailed cellular events involved in the remodeling process after microfat grafting and describe the long-term fate of adipose tissue and adipocytes. Understanding these events should help establish novel technologies to maximize and stabilize long-term results. In addition to the fragile nature of adipose tissue, a number of patient-derived or surgeon-dependent factors appear to affect clinical outcomes. We need to clarify how these affect not only tissue revascularization/regeneration but also tissue necrosis and the subsequent absorption/fibrosis of the microfat graft.

MATERIALS AND METHODS

Animal Models for Autologous Fat Grafting

Animals were cared for in accordance with our institutional guidelines. Eight-week-old BL6/Jjcl mice were purchased from Japan CLEA, Inc. (Tokyo, Japan). The mice were anesthetized with pentobarbital (50 mg/kg). The inguinal skin was incised and the subcutaneous inguinal fat pad (150 to 200 mg) was gently dissected and harvested. The fat pad was small, similar to the size of aspirated fat tissue used for clinical fat injection in humans. The fat pad was inserted through a 5-mm-long skin incision into a small pocket made under the scalp of the same mouse, followed by skin closure with a 7-0 nylon suture. The fat grafting was performed in 30 mice, which were killed after 0 (sham operation), 1, 2, 4, 8, or 12 weeks ($n = 5$ at each time point). After the scalp was incised, the grafted fat sample was harvested by careful removal from surrounding tissue and then weighed. The normalized sample weight ratio, which is the ratio of the harvested sample weight to the body weight, was used to evaluate the change in sample weight. Each harvested sample was fixed (Zinc Fixative; BD Biosciences, San Jose, Calif.) and embedded in paraffin for histologic assessment.

Histologic Assessment

After preparing 5-μm-thick sections of the harvested tissue samples, we performed immunostaining with the following primary antibodies: guinea pig anti-mouse perilipin (dilution, 1:200; Progen, Heidelberg, Germany), rat anti-mouse MAC-2 (dilution, 1:200; Cedarlane Corp., Burlington, Ontario, Canada), goat anti-mouse CD34 (dilution, 1:100; Santa Cruz Biotechnology, Santa Cruz, Calif.), rabbit anti-human Ki67 (clone SP6; dilution, 1:200; Thermo Fisher Scientific, Fremont, Calif.), and rabbit anti-mouse CD206 (dilution, 1:100; Santa Cruz Biotechnology). For double fluorescence staining, the following secondary antibodies were used: Alexa Fluor 488–conjugated goat anti-guinea pig immunoglobulin G (dilution, 1:200; Invitrogen, Carlsbad, Calif.), Alexa Fluor 568–conjugated donkey anti-rat immunoglobulin G (dilution, 1:200; Invitrogen), Alexa Fluor 488–conjugated donkey anti-goat immunoglobulin G (dilution, 1:200; Invitrogen), Alexa Fluor 594–conjugated donkey anti-rabbit immunoglobulin G (dilution, 1:200; Invitrogen), and Alexa Fluor 488–conjugated goat anti-rabbit immunoglobulin G (dilution, 1:200; Invitrogen). An isotype immunoglobulin G was used as a negative control for each immunostaining. Nuclei were stained with Hoechst 33342 (dilution, 1:200; Dojindo, Tokyo, Japan) and blood vessels were stained with isolectin 488 (dilution, 1:200; Invitrogen). The number of small adipocytes (perilipin-positive cells with a diameter <20 μm) was counted in at least four field images for each sample.

Statistical Analysis

The results are expressed as mean ± SEM. The Welch t test was used for all comparisons. Values of $p < 0.05$ were considered statistically significant.

RESULTS

Macroscopic and Weight Changes of Grafted Tissue Samples

The size and weight of the grafted fat tissue decreased over time (Fig. 1). [**See Figure, Supplemental Digital Content 1**, which shows immunohistology for viable adipocytes in transplanted

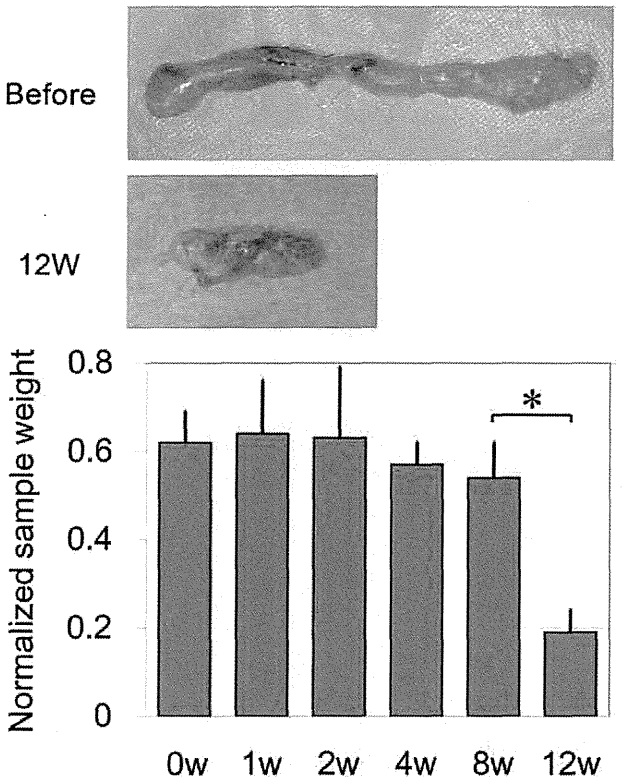

Fig. 1. Grafted fat tissue samples. (*Above*) Macroscopic views of grafted fat samples before and 12 weeks after grafting. (*Below*) Weight of grafted samples. The sample weight was normalized by dividing the sample weight by the body weight. The normalized weight ratio was significantly reduced at 12 weeks, compared with the ratio at baseline. Data are shown as mean ± SEM (*$p < 0.05$).

samples (complete version of Fig. 2), ***http://links.lww.com/PRS/A944***. Harvested tissue samples (before and 1, 2, 4, 8, and 12 weeks after grafting) were immunostained for perilipin (cytoplasm of viable adipocytes, green), MAC2 (monocytes/macrophages, red), and Hoechst 33342 (nuclei, blue). Rectangles in the low-magnification images (left column; yellow scale bars = 100 μm) were further magnified in the right column (white scale bars = 30 μm). Demarcation between the surviving and regenerating zone became clear at 1 week (dotted line); dead adipocytes (*) were perilipin-negative and surviving adipocytes were strongly positive for perilipin. Small preadipocytes with multiple intracellular lipid droplets (arrows) appeared around dead adipocytes at 2 to 4 weeks; the dead adipocytes were surrounded by a single layer of macrophages (red). Adipose regeneration was finished by 12 weeks, leaving large lipid drops (#) in the tissue.] The normalized sample weight ratio did not change significantly up to and including 8 weeks, but it exhibited a large decrease between 8 and 12 weeks. The mean normalized weight ratio at 12 weeks (0.19 ± 0.05, $n = 3$) was less than one-third of the ratio at baseline, before grafting (0.62 ± 0.07, $n = 3$).

Dynamic Adipose Tissue Remodeling after Grafting

Viable adipocytes and macrophages were visualized by immunohistochemistry staining for perilipin and MAC2, respectively (Fig. 2) (**see Figure, Supplemental Digital Content 1, *http://links.lww.com/PRS/A944***). At baseline, mature adipocytes (perilipin-positive) with relatively consistent size (70- to 120-μm diameter) and few macrophages ($MAC2^+$) were observed (Fig. 2, *above*). During the first week after fat grafting, many of the adipocytes died, likely because of ischemia as reported previously.[9] At 1 week, demarcation between the surviving superficial area (surviving zone) and the dead deeper area (regenerating or necrotizing zone) was very clear (Fig. 2, *second row*) (**see Figure, Supplemental Digital Content 1**, *second row*, ***http://links.lww.com/PRS/A944***) because dead adipocytes lost their perilipin stain completely by 1 week. Surviving adipocytes were located superficially below the tissue edge to a depth of 100 to 300 μm.

At 2 and 4 weeks after grafting, new adipocytes, which were strongly positive for perilipin and small (<30 μm), were frequently observed around dead adipocytes in the regenerating zone (Fig. 2, *third row*) (**see Figure, Supplemental Digital Content 1**, *third and fourth rows*, ***http://links.lww.com/PRS/A944***). These dead adipocytes were surrounded by a single layer of infiltrating macrophages. It was very easy to distinguish dead, shrinking (being absorbed) adipocytes from new, growing adipocytes; the former were perilipin-negative and surrounded by macrophages, whereas the latter were strongly positive for perilipin and frequently contained multiple intracellular lipid droplets.

At 8 weeks after grafting, adipogenesis was finishing and small dead adipocytes were still being absorbed or replaced with fibrotic material. (**See Figure, Supplemental Digital Content 1**, *fifth row*, ***http://links.lww.com/PRS/A944***.) At 12 weeks, adipogenesis was complete, and most of the living adipocytes appeared mature (Fig. 2, *below*) (**see Figure, Supplemental Digital Content 1**, *below*, ***http://links.lww.com/PRS/A944***). Absorption and fibrous replacement of small dead adipocytes were not yet finished and large lipid drops (accumulated dead adipocytes in the necrotizing zone) remained.

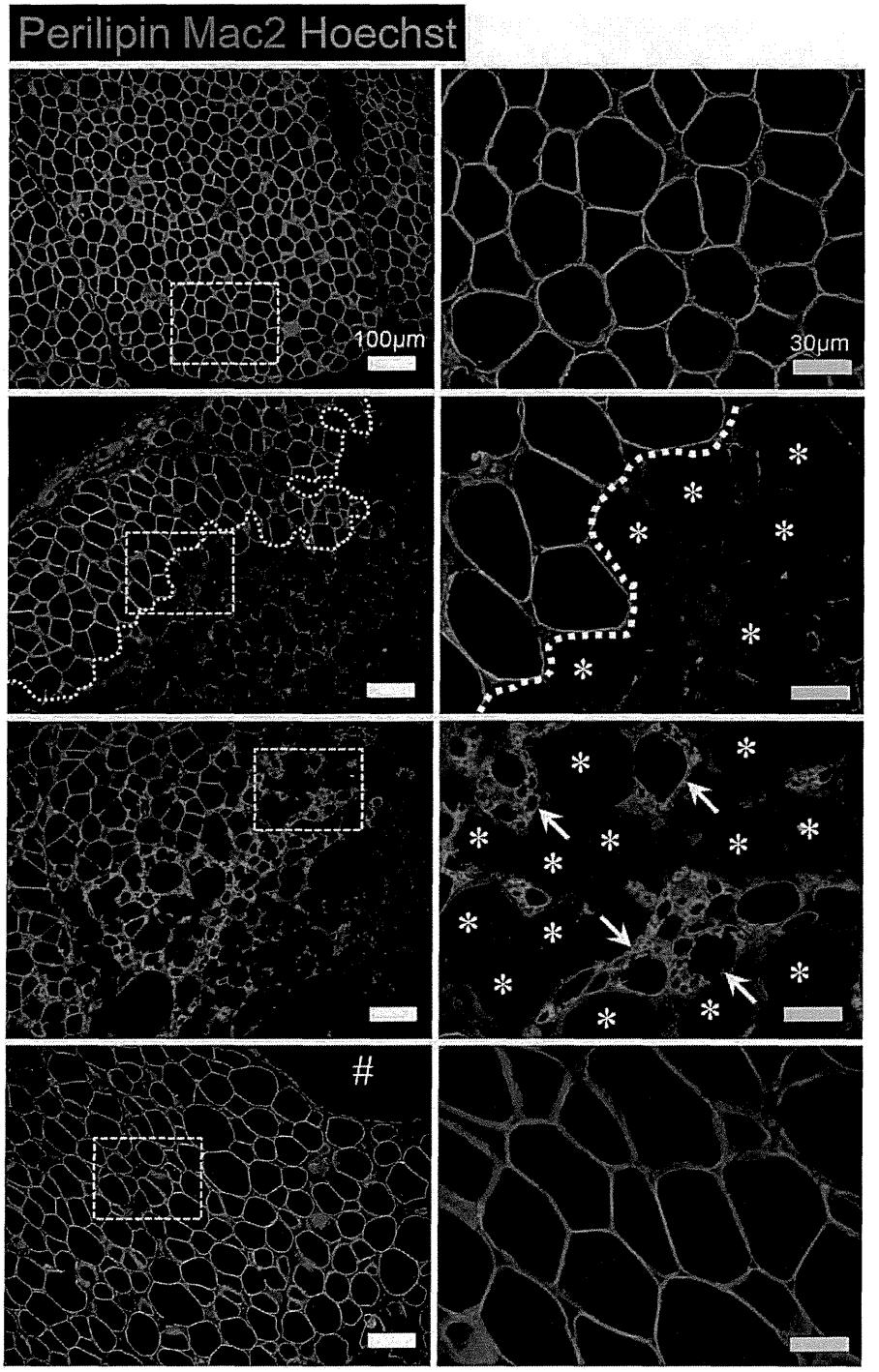

Fig. 2. Immunohistology for viable adipocytes in transplanted samples. Harvested tissue samples obtained before (*above*) and 1 week (*second row*), 4 weeks (*third row*), and 12 weeks (*below*) after grafting were immunostained for perilipin (cytoplasm of viable adipocytes, *green*), MAC2 (monocytes/macrophages, *red*), and Hoechst 33342 (nuclei, *blue*). Rectangles in the low-magnification images (*left column*; *white scale bars* = 100 μm) were further magnified in the *right column* (*yellow scale bars* = 30 μm). Demarcation between the surviving and regenerating zone became clear at 1 week (*dotted line*); dead adipocytes (*) were perilipin-negative and surviving adipocytes were strongly positive for perilipin. Small preadipocytes with multiple intracellular lipid droplets (*arrows*) appeared around dead adipocytes at 4 weeks; the dead adipocytes were surrounded by a single layer of macrophages (*red*). Adipose regeneration was complete at 12 weeks, leaving large lipid drops (#) in the tissue. (**See Figure, Supplemental Digital Content 1**, for the complete version of this figure, ***http://links.lww.com/PRS/A944***.)

Three Zones in Grafted Tissue: Surviving, Regenerating, and Necrotizing

Three zones were clearly demarcated at 4 weeks: surviving, regenerating, and necrotizing zones (Fig. 3). The most superficial layer (one to several rows of adipocytes) was the surviving zone. The intermediate layer, with a thickness of 600 to 1200 μm, was the regenerating zone, where many new adipocytes were observed adjacent to dead adipocytes. The innermost zone was the necrotizing zone, where new adipocytes were rare and inflammatory cells, oil drops, and fibrous areas were seen (Fig. 3, *above*). Interestingly, although most adipocytes had already died during the first week, the size of the grafted tissue did not change during the first 4 weeks. This indicates that the dead adipocytes generally maintained their size during this time, as the oil drops were slowly absorbed over a period of weeks or months, depending on their size. This seems to be a specific characteristic of mature adipocytes; these cells are extraordinarily large and most of their volume consists of lipid.

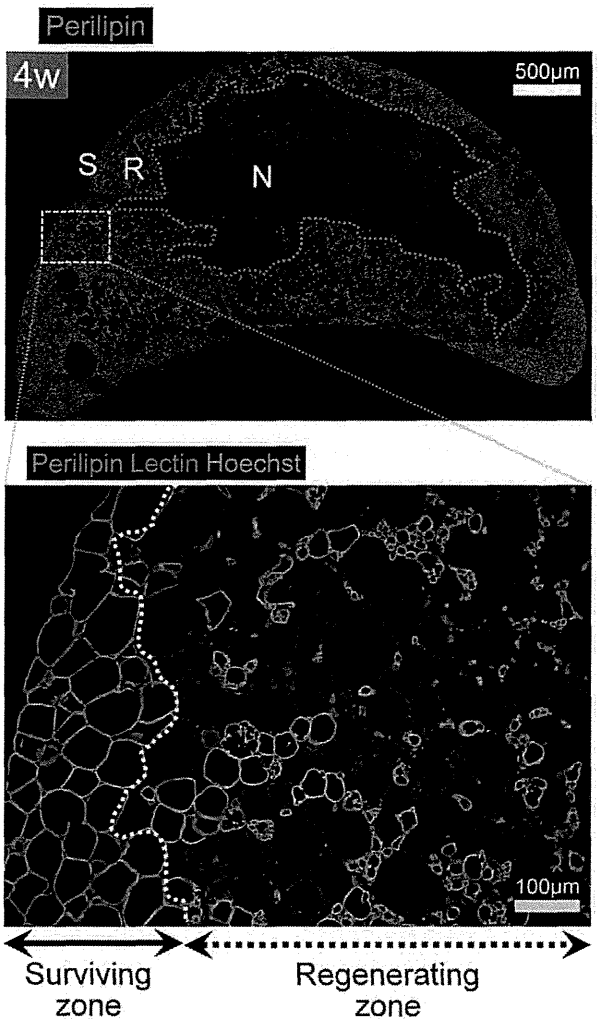

Fig. 3. Three demarcated zones in grafted adipose tissue. Immunohistology of a graft sample at 4 weeks showed demarcated surviving (*S*), regenerating (*R*), and necrotizing (*N*) zones. (*Above*) A low-magnification image of perilipin staining showed the necrotizing zone (*red dotted line*) with few perilipin-positive viable adipocytes (*white scale bar* = 500 μm). (*Below*) A high-magnification image of surviving and regenerating zones (*yellow scale bar* = 100 μm). The surviving zone comprising several layers of perilipin-positive viable adipocytes (*green*) was well demarcated from the regenerating zone (*white dotted line*). Many perilipin-positive small growing adipocytes were seen adjacent to perilipin-negative dark round areas (dead adipocytes not yet absorbed). Vascular endothelial cells and nuclei were stained with lectin (*red*) and Hoechst (*blue*).

Adipogenesis in the Regenerating Zone

The number of new (pre)adipocytes (small adipocytes strongly positive for perilipin), representing ongoing adipogenesis, was counted in immunohistochemical sections (Fig. 4). The number in the regenerating zone increased rapidly after grafting and peaked at 4 weeks. The number of new adipocytes was significantly higher at 1, 2, and 4 weeks than at baseline (0 weeks). Thereafter, the number declined to baseline by 12 weeks, suggesting that adipogenesis for remodeling was complete by 12 weeks.

Cells Surrounding Oil Drops

After adipocyte death during the first week, numerous dead adipocytes (oil droplets with the

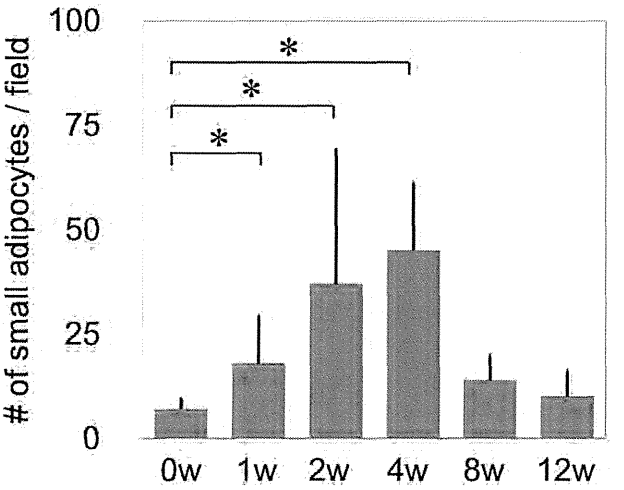

Fig. 4. Sequential changes in number of new adipocytes. Newly born adipocytes (preadipocytes), which are small (<20 μm) and strongly positive for perilipin, were counted. Adipogenesis peaked at 4 weeks and returned to baseline level by 12 weeks (*$p < 0.05$).

size of adipocytes) were seen in the regenerating and necrotizing zones. Every oil drop was surrounded by $MAC2^+/CD206^-$ macrophages in the regenerating zone at 2 weeks (Fig. 5, *above*), suggesting that these were inflammatory M1 macrophages scavenging the lipid content. The macrophages formed a single circular layer around each oil drop. By contrast, many macrophages surrounding oil drops in the necrotizing zone were $MAC2^+/CD206^+$, suggesting that they were antiinflammatory M2 macrophages. Some of the M2 macrophages were also positive for CD34. Interestingly, the macrophages in the necrotizing zone formed a single circular layer around some oil drops and multiple layers around others.

In the superficial part of the regenerating zone, adipogenesis appeared to be complete at 8 weeks, although some large oil drops remained (Fig. 5, *center*). These oil drops were surrounded by single-layered macrophages. At 12 weeks, adipogenesis appeared to be complete in the border area between the regenerating and necrotizing zone, but oil absorption or replacement with fibrosis was still occurring (Fig. 5, *below*). Oil droplets with the size of adipocytes that were not yet completely absorbed were surrounded by multilayered M2 macrophages (Fig. 5, *below*), whereas some oil droplets were completely absorbed, leaving only the multilayered M2 macrophages (Fig. 5, *below*). These findings likely represent the process of oil drop replacement by fibrosis, mediated by M2 macrophages. These phenomena were not seen in the surviving or superficial regenerating zone but observed only in and around the necrotizing zone. Histopathologic findings shown in Figures 2 through 5 are summarized in Table 1.

Proliferating Cells during the Adipose Remodeling Process

Sequential changes of the number and type of proliferating cells were examined using immunohistochemical sections for Ki67 (Table 2). Although cell proliferation was generally not active until 1 week, numerous proliferative cells were observed in the regenerating and necrotic zones at 2 and 4 weeks. The proliferating cells were predominantly $MAC2^+$ macrophages, and other proliferating cells were $CD34^+$ cells; most of the $CD34^+$ cells were likely adipose stem/progenitor/stromal cells. At 8 weeks, proliferating cells were rare in the regenerating zone, but there were still many proliferating cells in the necrotizing zone, suggesting that remodeling in the regenerating zone was finishing at 8 weeks. Thereafter, the number of proliferating cells in the necrotizing zone decreased over time, but some proliferating cells remained in the necrotizing zone even at 12 weeks, suggesting that dynamic cellular events, such as lipid absorption or fibrosis replacement, were still ongoing.

DISCUSSION

To experimentally simulate human microfat grafting, we selected a mouse model of an autologous fat graft with the inguinal fat pad as donor tissue and the head as the recipient site. The inguinal fat pad is the approximate size of a typical human microfat injection (150 to 200 mg) and it is easy to prepare consistently, although we did not use aspirated fat tissue and it may interfere with the outcomes. Another limitation is that the mouse has little subcutaneous fat tissue and thus the recipient condition is not comparable with that in humans. As the scalp is immobile, it is an ideal location for ensuring postoperative immobilization.

This study reconfirmed the adipocyte replacement theory that we reported previously[9] and presented further details regarding adipocyte replacement with new-generation cells. Demarcation of the surviving zone (100 to 300 μm thick) from the regenerating zone (600 to 1200 μm thick) became clear at 1 week, and new adipocytes (preadipocytes) with intracellular multiple lipid droplets appeared around the dead adipocytes at 1 to 2 weeks, surrounded by a single layer of M1 macrophages (producing a crown-like structure). Adipose stem/progenitor/stromal cells are known to be located perivascularly along the capillaries between adipocytes.[16] We previously showed that adipose stem/progenitor/stromal cells are exceedingly tolerant to ischemia, allowing them to remain alive for up to 3 days under conditions of severe hypoxia.[9] Perivascular adipose stem/progenitor/stromal cells are activated by the death of adjacent adipocytes and give rise to new adipocytes in the regenerating zone if the microenvironment, including the vascularity and oxygen tension, is improved within 3 days after grafting. If capillary growth from surrounding intact tissue does not reach the area and the microenvironment does not improve sufficiently within 3 days, the adipose stem/progenitor/stromal cells will also die, thereby aborting the regenerative process. This area will then become the necrotizing zone.

Interestingly, although most of the adipocytes died after fat grafting, the graft size and weight

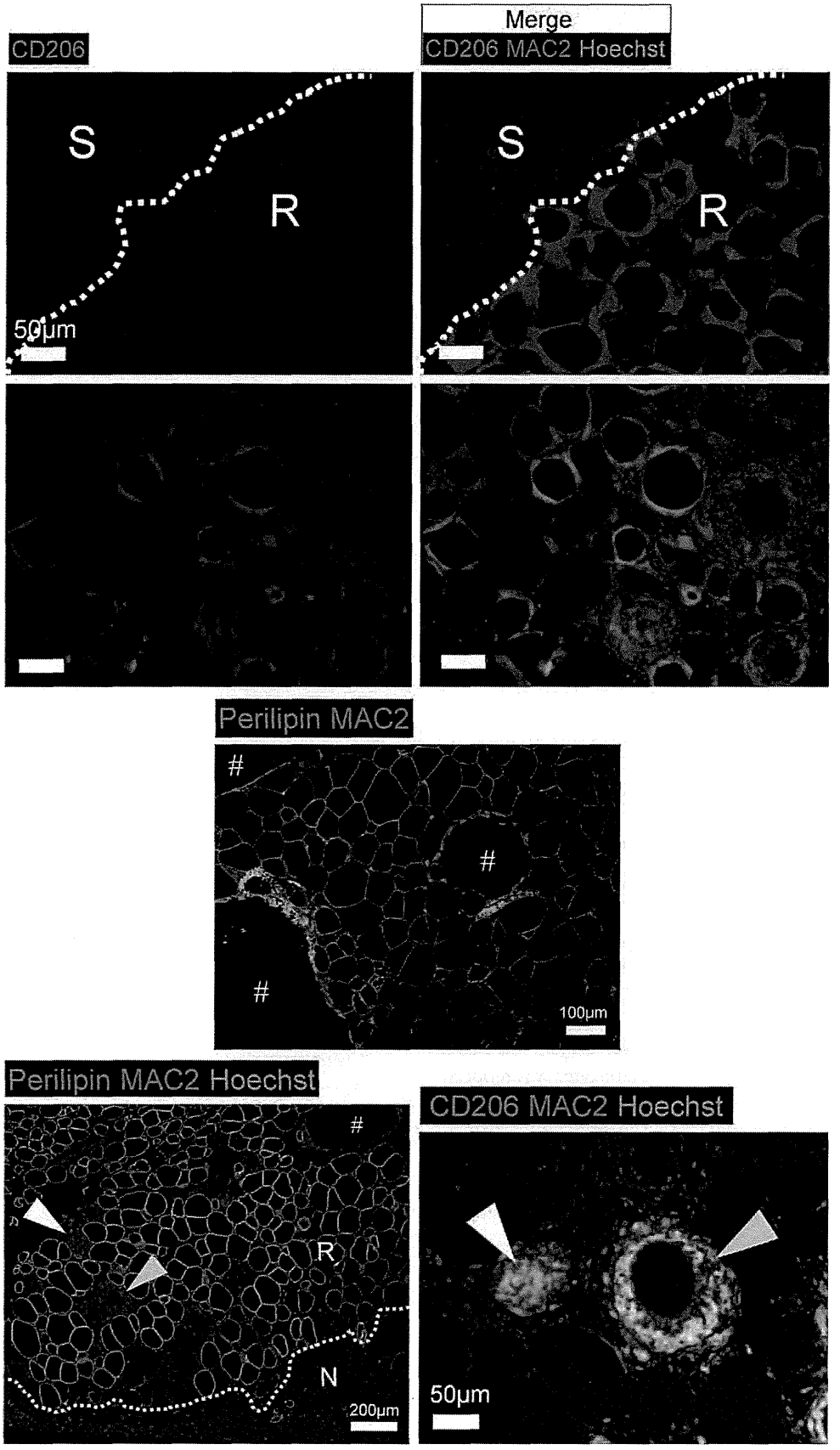

Fig. 5. Histology for macrophages working in adipose remodeling. Macrophages were visualized with immunostaining for MAC2. (*Above*) At 2 weeks, in the regenerating zone (*R*) demarcated

Table 1. Summary of Histopathologic Findings after Fat Grafting

	General Comments	Surviving Zone	Regenerating Zone	Necrotic Zone
1 wk	Surviving zone is clearly demarcated from other zones where ischemic degeneration is seen. As regeneration is not obvious, regenerating zone is not yet clearly demarcated from necrotizing zone.	Matured adipocytes remain intact (keeping perilipin expression and round shape).	All adipocytes died (lost perilipin expression) and remain as adipocyte-sized oil droplets. Regenerative events are not yet obvious.	All adipocytes died (lost perilipin expression).
2–4 wk	Regeneration is seen and peaked at 4 wk. Scavenging dead adipocytes by infiltrated macrophages progress simultaneously. The border between regenerating zone and necrotizing zone becomes clear.	Same as above.	Numerous growing preadipocytes (small, perilipin-positive, and containing multiple tiny lipid droplets) emerge between crown-like structures (dead adipocytes surrounded by M1 macrophages).	Dead adipocytes and numerous inflammatory cells (lymphocytes and macrophages) are observed, but no regenerative changes such as new preadipocytes are seen. A numerous number of M2 macrophages are seen, as are M1 macrophages. Large oil drops (derived from many dead adipocytes) surrounded by macrophages are seen.
8 wk	Most new adipocytes get matured and the border between surviving zone and regenerating zone become unclear.	Same as above.	Most of the new adipocytes get matured and the number of small adipocytes is small.	No adipogenesis is seen. Many small and large oil drops were seen along with numerous inflammatory cells. Some oil drops are surrounded by multilayered M1 and M2 macrophages, suggesting that fibrogenesis is in progress with scavenging.
12 wk	The total size of the tissue becomes small, probably resulting from accelerated oil absorption. Regeneration appears completed in the regenerating zone, although stabilization of the tissue is not yet completed in the central necrotizing zone.	Same as above.	Tissue is filled with matured adipocytes and appears intact.	The number of small oil drops is reduced, but many large oil drops remain with surrounding inflammatory cells, suggesting that the stabilization process will further need a long time until completed.

did not change significantly until 8 weeks. This observation can be explained by the immunohistologic findings at 2 and 4 weeks. Numerous small oil droplets (adipocyte size; derived from a single dead adipocyte) and large drops (from multiple dead adipocytes) surrounded by macrophages were histologically detected at 1 week and later. However, the oil drops were only slowly absorbed, so they continued to contribute volume and weight to the sample for weeks or even months. Thus, the dead adipocytes functioned as spacers to maintain the grafted tissue volume during the remodeling process; this phenomenon appears to

Fig. 5. (*Continued*) from the surviving zone (*S*), dead adipocytes were surrounded by $MAC2^+CD206^-$ M1 macrophages (*scale bar* = 50 μm). $MAC2^+CD206^+$ M2 macrophages were observed in the necrotizing zone and M1 macrophages. (*Center*) At 8 weeks, the number of perilipin-positive small adipocytes was reduced, suggesting that the regeneration was finishing (*scale bar* = 100 μm). Groups of dead adipocytes formed oil drops (#), which were surrounded by macrophages. (*Below*) At 12 weeks, in border areas between the regenerating (*R*) and necrotizing (*N*) zones, adipogenesis appeared to be complete, but oil absorption and fibrous replacement were still ongoing. In addition to large oil drops (#) surrounded by macrophages, adipocyte-sized macrophage clusters were observed with (*yellow arrowheads*) or without (*white arrowheads*) lipid droplets inside (*left*; *scale bar* = 200 μm). The lipid droplet–containing macrophage cluster was composed of an innermost single layer of M1 macrophages ($MAC2^+CD206^-$) and outer multilayered M2 macrophages ($MAC2^+CD206^-$) (*right*; *scale bar* = 50 μm). It is suspected that M2 macrophages appeared in unfavorable conditions where adipocyte regeneration failed and fibrous replacement of the space was needed.

Table 2. Type and Localization of Proliferating Cells

	Surviving Zone	Regenerating Zone	Necrotizing Zone
Before	–	–	–
1 wk	–	+ ($MAC2^+ > CD34^+$)	–
2 wk	–	+++ ($MAC2^+ > CD34^+$)	+++ ($MAC2^+ > CD34^+$)
4 wk	–	+++ ($MAC2^+ > CD34^+$)	+++ ($MAC2^+ > CD34^+$)
8 wk	–	–	++ ($MAC2^+ > CD34^+$)
12 wk	–	–	+ ($MAC2^+ > CD34^+$)

facilitate the dynamic adipocyte replacement by activated adipose stem/progenitor/stromal cells.

Our results suggest that the first 3 months after transplantation is a period of tissue repair and that adipogenesis will not occur after this period. After the initial ischemic damage to the tissue, inflammatory cells infiltrated the grafted tissue, initially entering the regenerating zone and then the necrotizing zone. In the regenerating zone, adipogenesis and angiogenesis progressed and many of the dead adipocytes were replaced with next-generation adipocytes, which probably originated from tissue-resident adipose stem/progenitor/stromal cells. In parallel with the regenerating events, stabilizing events, such as lipid absorption (phagocytosis) and lipid replacement with scar tissue (fibrosis), occurred. Both the regenerating and stabilizing processes progressed from the superficial layers of the regenerating zone to the deeper layers over the first 3 months. Although the regeneration process peaked at 4 weeks and was complete by 3 months, the stabilizing process was not finished at 3 months. The stabilizing process may persist for at least several more months, as suggested by clinical observations that volume reduction after fat grafting continues until the end of the first year. Our findings also showed that adipocyte-sized oil droplets were absorbed or temporarily filled with multilayered M2 macrophages, producing fibrosis, but substantially larger oil drops may form oil cysts in several months and remain permanently.

Immunohistologic assessment for Ki67 demonstrated the presence of proliferative cells during the remodeling process. $Ki67^+/CD34^+$ cells (proliferating more) appeared at 1 week, increased in number at 2 to 4 weeks in the regenerating zone, and thereafter decreased gradually, suggesting that these cells are associated with adipogenesis/angiogenesis. However, a majority of the proliferating cells in the repair period were not adipose stem/progenitor/stromal cells, but were $MAC2^+$ monocytes/macrophages, which were seen in both the regenerating and necrotic zones. $Ki67^+/MAC2^+$ cells appeared as single or multiple layers of cells surrounding oil droplets, suggesting that M1 and M2 macrophages continued to proliferate during the stabilizing process. Proliferating anti-inflammatory M2 macrophages originating locally have been reported in various inflammatory conditions.[17–20] The number of $Ki67^+/MAC2^+$ cells decreased gradually after 4 weeks, reflecting the changing dynamics of the remodeling process.

Our results suggested that two different types of macrophages, M1 and M2 macrophages, may have distinct roles: phagocytosis and fibrosis (or managing the dead space), respectively. M2 macrophages appeared at later stages than M1 macrophages, and they were frequently observed in deeper zones, suggesting that M2 macrophages have a biological role in working under unfavorable microenvironments, such as severe ischemia. Two types of small oil droplets were observed: adipocyte-sized oil droplets surrounded by a single layer of M1 macrophages and smaller oil droplets surrounded by multiple, stratified macrophages (an inner single layer of M1 macrophages and outer multiple layers of M2 macrophages). These findings suggest that M2 macrophages contribute to filling the dead space with fibrous tissue in parallel with lipid absorption in the deeper regenerating and necrotic zones.

Based on the results of the present study, we have summarized the fate of adipocytes in grafted adipose tissue in Figure 6. The fate of these cells depends on the microenvironment (such as vascularity and oxygenation) in which each adipocyte is placed. Adipocytes remain alive in the surviving zone, whereas they die shortly after grafting in the regenerating and necrotizing zones. On adipocyte death, adjacent adipose stem/progenitor/stromal cells are activated and begin to differentiate into adipogenic lineage cells in the regenerating zone, whereas adipose stem/progenitor/stromal cells also die in the necrotizing zone. Dead adipocytes under better conditions in the regenerating zone are phagocytized by M1 macrophages and are successfully replaced by new adipocytes without residual fibrosis. By contrast, dead adipocytes under worse conditions in the regenerating or necrotizing zones are surrounded by M1 and M2 macrophages; oil absorption by M1 macrophages occurs along with fibrous replacement of the space (fibrogenesis) by M2 macrophages. In the necrotizing zone, many large oil drops, derived from a group of dead adipocytes, are formed, which are also surrounded by M1 and M2 macrophages. The time required for oil absorption is generally proportional to the oil drop diameter, and oil absorption and fibrous replacement are not complete within 3 months for large oil drops. For these drops, complete absorption of the oil content may occur for many more months or a cystic wall may form that prohibits total absorption.

CONCLUSIONS

This study revealed the underlying mechanisms of successful (regeneration) and unsuccessful (cicatrization) tissue remodeling, which should facilitate the future development of strategies to improve the clinical outcome of fat grafting. Grafted fat tissue undergoes degeneration during

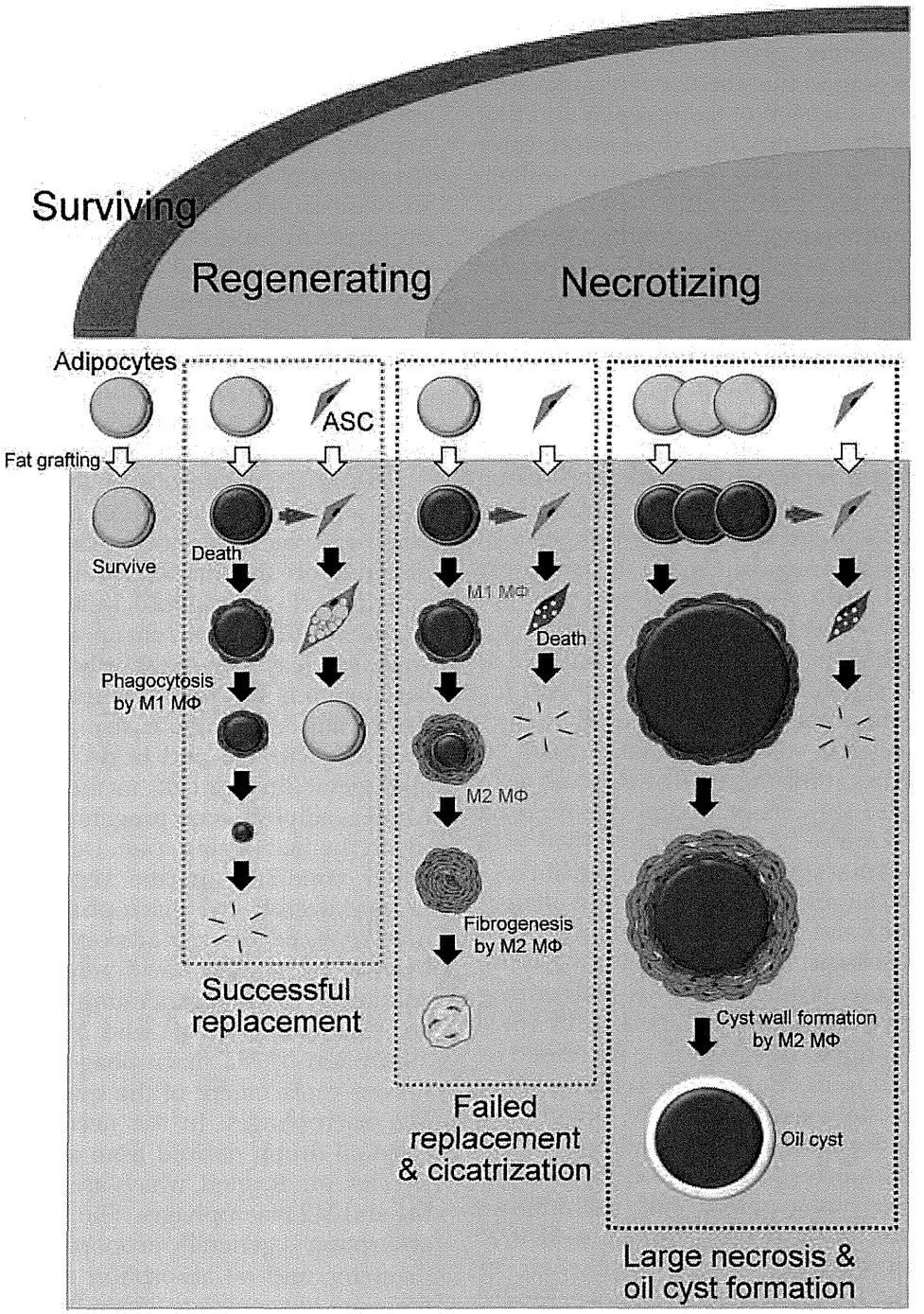

Fig. 6. Conclusive schema for the fate of adipocytes in grafted fat. During the first 3 months of adipose tissue remodeling, transplanted adipocytes have differential fates depending on their microenvironments. In this schema, complex cellular events are simplified and the adipocyte fate is categorized into four patterns: survival, successful regeneration, failed regeneration (cicatrization), and oil cyst formation. Cicatrization and oil cyst formation are often not complete at 3 months. *ASC*, adipose stem/progenitor/stromal cells.

the first week, and regeneration peaked at 4 weeks. Adipose tissue-resident progenitor cells contribute to the regeneration, and M1 and M2 macrophages play pivotal roles in phagocytosis and cicatrization, respectively, in the regenerating and necrotizing zones. The stabilization process after failed regeneration appears to persist for a long time. The size of the necrotizing zone depends predominantly

on the size of the grafted tissue and the microenvironment into which it is placed. Necrotic zones will eventually be absorbed, filled with fibrous tissue, or become problematic cysts. To minimize the size of the necrotic zone, liposuction and reinjection procedures could be improved by preparing grafts with better viability and an appropriate size, maximizing the contact surface of the grafts by ideal distribution, and placing the grafts in areas with high vascularity. Stabilization of the grafted fat may not occur until many months after complete regeneration at 3 months, thereby emphasizing the importance of long-term follow-up to thoroughly evaluate the clinical results of micro–fat-grafting procedures.

Kotaro Yoshimura, M.D.
Department of Plastic Surgery
University of Tokyo School of Medicine
7-3-1, Hongo, Bunkyo-Ku
Tokyo 113-8655, Japan
kotaro-yoshimura@umin.ac.jp

REFERENCES

1. Coleman SR. Structural fat grafting: More than a permanent filler. *Plast Reconstr Surg.* 2006;118(Suppl):108S–120S.
2. Yoshimura K, Sato K, Aoi N, et al. Cell-assisted lipotransfer for cosmetic breast augmentation: Supportive use of adipose-derived stem/stromal cells. *Aesthetic Plast Surg.* 2008;32:48–55.
3. Khouri RK, Eisenmann-Klein M, Cardoso E, et al. Brava and autologous fat transfer is a safe and effective breast augmentation alternative: Results of a 6-year, 81-patient, prospective multicenter study. *Plast Reconstr Surg.* 2012;129:1173–1187.
4. Del Vecchio D, Rohrich RJ. A classification of clinical fat grafting: Different problems, different solutions. *Plast Reconstr Surg.* 2012;130:511–522.
5. Yoshimura K, Shigeura T, Matsumoto D, et al. Characterization of freshly isolated and cultured cells derived from the fatty and fluid portions of liposuction aspirates. *J Cell Physiol.* 2006;208:64–76.
6. Eto H, Suga H, Matsumoto D, et al. Characterization of structure and cellular components of aspirated and excised adipose tissue. *Plast Reconstr Surg.* 2009;124:1087–1097.
7. Suga H, Eto H, Aoi N, et al. Adipose tissue remodeling under ischemia: Death of adipocytes and activation of stem/progenitor cells. *Plast Reconstr Surg.* 2010;126:1911–1923.
8. Suga H, Eto H, Shigeura T, et al. IFATS collection: Fibroblast growth factor-2-induced hepatocyte growth factor secretion by adipose-derived stromal cells inhibits postinjury fibrogenesis through a c-Jun N-terminal kinase-dependent mechanism. *Stem Cells* 2009;27:238–249.
9. Eto H, Kato H, Suga H, et al. The fate of adipocytes after nonvascularized fat grafting: Evidence of early death and replacement of adipocytes. *Plast Reconstr Surg.* 2012;129:1081–1092.
10. Aiba-Kojima E, Tsuno NH, Inoue K, et al. Characterization of wound drainage fluids as a source of soluble factors associated with wound healing: Comparison with platelet-rich plasma and potential use in cell culture. *Wound Repair Regen.* 2007;15:511–520.
11. Suga H, Eto H, Aoi N, et al. Adipose tissue remodeling under ischemia: Death of adipocytes and activation of stem/progenitor cells. *Plast Reconstr Surg.* 2010;126:1911–1923.
12. Eto H, Suga H, Inoue K, et al. Adipose injury-associated factors mitigate hypoxia in ischemic tissues through activation of adipose-derived stem/progenitor/stromal cells and induction of angiogenesis. *Am J Pathol.* 2011;178:2322–2332.
13. Yoshimura K, Suga H, Eto H. Adipose-derived stem/progenitor cells: Roles in adipose tissue remodeling and potential use for soft tissue augmentation. *Regen Med.* 2009;4:265–273.
14. Yoshimura K, Eto H, Kato H, Doi K, Aoi N. In vivo manipulation of stem cells for adipose tissue repair/reconstruction. *Regen Med.* 2011;6(Suppl):33–41.
15. Nishimura S, Manabe I, Nagasaki M, et al. Adipogenesis in obesity requires close interplay between differentiating adipocytes, stromal cells, and blood vessels. *Diabetes* 2007;56:1517–1526.
16. Traktuev DO, Merfeld-Clauss S, Li J, et al. A population of multipotent CD34-positive adipose stromal cells share pericyte and mesenchymal surface markers, reside in a periendothelial location, and stabilize endothelial networks. *Circ Res.* 2008;102:77–85.
17. Anthony RM, Rutitzky LI, Urban JF Jr, et al. Protective immune mechanisms in helminth infection. *Nat Rev Immunol.* 2007;7:975–987.
18. Siracusa MC, Reece JJ, Urban JF Jr, et al. Dynamics of lung macrophage activation in response to helminth infection. *J Leukoc Biol.* 2008;84:1422–1433.
19. Chorro L, Sarde A, Li M, et al. Langerhans cell (LC) proliferation mediates neonatal development, homeostasis, and inflammation-associated expansion of the epidermal LC network. *J Exp Med.* 2009;206:3089–3100.
20. Jenkins SJ, Ruckerl D, Cook PC, et al. Local macrophage proliferation, rather than recruitment from the blood, is a signature of TH2 inflammation. *Science* 2011;332:1284–1288.

Chronic Inflammation and Progressive Calcification as a Result of Fat Necrosis: The Worst Outcome in Fat Grafting

Kazuhide Mineda, M.D.
Shinichiro Kuno, M.D.
Harunosuke Kato, M.D.
Kahori Kinoshita, M.D.
Kentaro Doi, M.D.
Ichiro Hashimoto, M.D.
Hideki Nakanishi, M.D.
Kotaro Yoshimura, M.D.

Tokyo and Tokushima, Japan

Background: Autologous fat injection into the breast has been performed widely for breast augmentation and reconstruction because of recent technical and scientific advancements. However, it is important to learn what occurs and how problematic it can be if fat grafting is not conducted appropriately.
Methods: Oil cysts were explanted from three subjects who underwent cosmetic fat grafting to the breast 2, 4, and 6 years previously. The oil cyst samples were examined histopathologically. Computed tomographic, magnetic resonance imaging, and mammographic images obtained sequentially after fat grafting were also analyzed.
Results: The cyst wall consisted of innermost and outermost fibrous layers and intermediate tissue that contained the regular adipose portion, a degenerated adipose portion, and a fibrous area. Eggshell-like macrocalcifications were seen in the inner surface. Numerous inflammatory cells, mainly $MAC2^+/CD206^+$ anti-inflammatory M2 macrophages, were observed in the degenerated adipose portion. Oil cysts with a longer history showed more calcifications in the innermost layer and a larger fibrous area adjacent to the degenerated fat portion than those with a shorter history. These histopathologic findings and clinical computed tomographic images revealed that oil cysts continued to be inflammatory and calcifications continued to develop over several years.
Conclusions: After fat necrosis, long-term chronic inflammation persists and calcification seems to progress without limits. Oil cysts are the worst outcome of fat grafting and must be avoided by standardizing meticulous injection techniques. (*Plast. Reconstr. Surg.* 133: 1064, 2014.)
CLINICAL QUESTION/LEVEL OF EVIDENCE: Therapeutic, V.

THERAPEUTIC 5

Autologous fat injection has become a fascinating modality for tissue repair and reconstruction, because adipose tissue contains many stem cells that may revitalize pathologic tissues, such as irradiated tissue.[1] Recent technical and scientific advances in fat-grafting procedures and concepts have reduced clinical complications and improved predictability,[2,3] resulting in relative acceptance of large-volume fat grafting even to the breast.[4–9] However, central fat necrosis certainly occurs when fat is grafted as a large (>3 mm) drop and microenvironments around grafted fat are not properly improved during the first 3 days.[10,11] Thus, we need to learn more clearly what occurs and how problematic it is if fat grafting is not performed appropriately.[12–14]

Oil cysts and calcifications caused by fat necrosis have been reported frequently.[15–18] Microcalcification or macrocalcification was detected in 25 percent of cases at 16.2 ± 13.5 months after lipoinjection into the breast,[16] although another study

From the Department of Plastic Surgery, University of Tokyo School of Medicine; and the Department of Plastic Surgery, University of Tokushima School of Medicine.
Received for publication July 22, 2013; accepted October 16, 2013.

DOI: 10.1097/PRS.0000000000000097

Disclosure: *The authors have no conflict of interest to declare.*

Supplemental digital content is available for this article. Direct URL citations appear in the text; simply type the URL address into any Web browser to access this content. Clickable links to the material are provided in the HTML text of this article on the *Journal*'s Web site (www.PRSJournal.com).

reported that microcalcification occurs in only 3.9 percent of patients.[17] Gosset et al.[18] reported that mammograms detected microcalcifications in 19 percent and magnetic resonance imaging found cystic lesions in 47 percent. However, it remains unknown how and when oil cysts and calcifications are formed and how surgeons can avoid or treat them.

In this study, we investigated patients with complications after fat grafting to the breast for cosmetic augmentation; patients with multiple oil cysts presented the most severe symptoms. We carefully examined histologic samples of removed oil cysts and analyzed long-term images such as mammograms and computed tomographic scans.

PATIENTS AND METHODS

Oil Cysts Removed from Patients Who Had Undergone Fat Grafting to the Breast

Oil cysts were removed from three women (cases 1, 2, and 3) (Table 1) who had undergone bilateral cosmetic breast augmentation with autologous fat injections at unknown cosmetic surgery clinics in Japan 2, 4, or 6 years ago, respectively. None of them has any children or a family history of breast cancer. They became aware of subcutaneous nodules with abnormal symptoms such as tenderness and contracture in both breasts and visited our hospital. Computed tomographic or magnetic resonance imaging was performed preoperatively.

Macroscopic and Stereomicroscopic Examination

At the time of removal of oil cysts, the inner content and the wall structure were photographed and evaluated macroscopically and stereomicroscopically.

Histologic Examination

All tissue samples removed were fixed (IHC Zinc Fixative; BD Biosciences, San Diego, Calif.) and embedded in paraffin wax. The samples were sectioned at 5 μm and subjected to the following staining procedures. Hematoxylin and eosin staining was performed for basic screening, whereas von Kossa staining and Alizarin Red S staining were conducted to visualize calcifications in black and red, respectively. For immunohistochemistry, the following primary antibodies were used: guinea pig anti-perilipin antibody (Progen, Heidelberg, Germany) to stain viable adipocytes, rat anti–MAC2 antibody (Cedarlane Laboratories, Burlington, Ontario, Canada) to stain macrophages, goat anti-CD34 antibody (Santa Cruz Biotechnology, Inc., Santa Cruz, Calif.) to stain adipose-derived stromal cells and vascular endothelial cells, and mouse anti-CD206 antibody (Santa Cruz Biotechnology) to stain anti-inflammatory M2 macrophages. Isotypic antibodies were used as a negative control for each immunostaining. For visualization, Alexa Fluor 488– or Alexa Fluor 568–conjugated secondary antibodies (Molecular Probes, Carlsbad, Calif.) were used. Vessels (vascular endothelial cells) were stained with Alexa Fluor 594–conjugated isolectin GS-IB_4 (Molecular Probes) and nuclei were stained with Hoechst 33342 (Dojindo, Kumamoto, Japan).

Long-Term Follow-Up Analyses: Computed Tomographic and Mammographic Images

We also analyzed sequential computed tomographic and mammographic images taken from patients who underwent fat injections to the breast and were followed over several years.

RESULTS

Preoperative Imaging Findings

Using computed tomography or magnetic resonance imaging, oil cysts were detected in all three cases; eggshell-like calcifications were detected on computed tomographic images, which were diagnosed as benign lesions resulting from fat necrosis. Preoperative computed tomography or magnetic resonance imaging of cases 1 through 3 are shown in **Figures, Supplemental Digital Content 1 through 3, *http://links.lww.com/PRS/A964*, *http://links.lww.com/PRS/A965*,** and **http://links.lww.com/PRS/A966**, respectively. See Appendix for details.

In case 1, preoperative computed tomography showed that there was a single large calcified oil cyst under each mammary gland, and it was suspected that 100 to 200 ml of fat tissue had been

Table 1. Patient Data from Histologic Samples

Case	Age (yr)	Postoperative Period (yr)	Injection Material	Findings
1	24	2	Autologous fat	Oil cysts, calcifications
2	30	4	Autologous fat	Oil cysts, calcifications
3	30	6	Autologous fat	Oil cysts, calcifications

introduced in a bolus injection before. (**See Figure, Supplemental Digital Content 1**, *B*, ***http://links.lww.com/PRS/A964***.) In case 2, three-dimensional computed tomography clearly indicated two large lumps with eggshell-like calcification below the mammary gland on each side. (**See Figure, Supplemental Digital Content 2**, *B*, ***http://links.lww.com/PRS/A965***.) Preoperative magnetic resonance imaging scan of case 3 showed multiple oil cysts, and the largest was located below the left mammary gland. (**See Figure, Supplemental Digital Content 3**, *B*, ***http://links.lww.com/PRS/A966***.)

Macroscopic and Stereomicroscopic Findings

In all cases, the removed oil cysts were filled with muddy contents, caused by fat necrosis (Fig. 1, *left*). Examinations under a stereomicroscope showed that the cyst wall had two white fibrous layers, between which a yellowish softer layer was observed. Scaly calcifications were observed on the inner surface of the wall (Fig. 1, *right*). Detailed macroscopic and microscopic findings of cases 1 through 3 are shown in **Figures, Supplemental Digital Content 1 through 3**, ***http://links.lww.com/PRS/A964***, ***http://links.lww.com/PRS/A965***, and ***http://links.lww.com/PRS/A966***, respectively.

Histopathology of Oil Cyst Walls

The oil cyst walls commonly had two fibrous layers as the innermost and outermost layers (Fig. 2, *above*). (**See Figures, Supplemental Digital Content 2**, *D*, ***http://links.lww.com/PRS/A965***, and **Supplemental Digital Content 3**, *C* and *D*, ***http://links.lww.com/PRS/A966***.) Between the two fibrous layers, we observed healthy appearing adipose tissue, degenerated adipose tissue, and connective tissue (Fig. 2, *center* and *below, left*). Some part of the adipose layer contained round adipocytes with strong expression of perilipin, blood vessels, and $CD34^+$ adipose-derived stromal cells, suggesting that it was close to healthy adipose tissue (Fig. 2, *below, right*). In contrast, the other part of the adipose layer was degenerated adipose tissue, which had irregularly shaped adipocytes weakly positive for perilipin, oil droplets with no expression of perilipin, and some fibrous areas (Fig. 2, *below, left*, and Fig. 3, *left*). (**See Figure, Supplemental Digital Content 3**, *E*, ***http://links.lww.com/PRS/A966***.) Various inflammatory cells, including lymphocytes and macrophages, had infiltrated into the degenerated part.

The degenerated fat portion contained a fibrous area where a number of small oil droplets (dead adipocytes) were present (Fig. 2, *above*, and Fig. 3, *left*). Those oil drops were surrounded by inflammatory cells, predominantly $MAC2^+$ macrophages (Fig. 3, *left*). Most of the macrophages were found to be $CD206^+$, indicating that they were anti-inflammatory M2 macrophages (Fig. 3, *right*). The patient in case 3, who had the longest follow-up after fat injection (6 years), showed a large area of fibrosis in the intermediate layer, suggesting that the degenerated fat portion may become fibrotic over time and that M2 macrophages may contribute to the fibrogenesis. Von Kossa and Alizarin Red S staining was performed to evaluate the degree and location of calcifications. All oil cysts showed calcifications localized in the innermost

Fig. 1. Macroscopic and stereomicroscopic appearance of an oil cyst in case 2. Fat grafting was performed 4 years earlier and multiple cysts were left in both breasts. (**See Figure, Supplemental Digital Content 2, *http://links.lww.com/PRS/A965***.) (*Left*) Macroscopically, the oil cyst was filled with muddy content, caused by fat necrosis, and calcified scales were seen on the inner surface of the cyst wall. (*Right*) Stereomicroscopically, the cyst wall had two white fibrous layers, between which a yellowish softer layer was observed. The *arrowhead* shows a calcified scale on the wall.

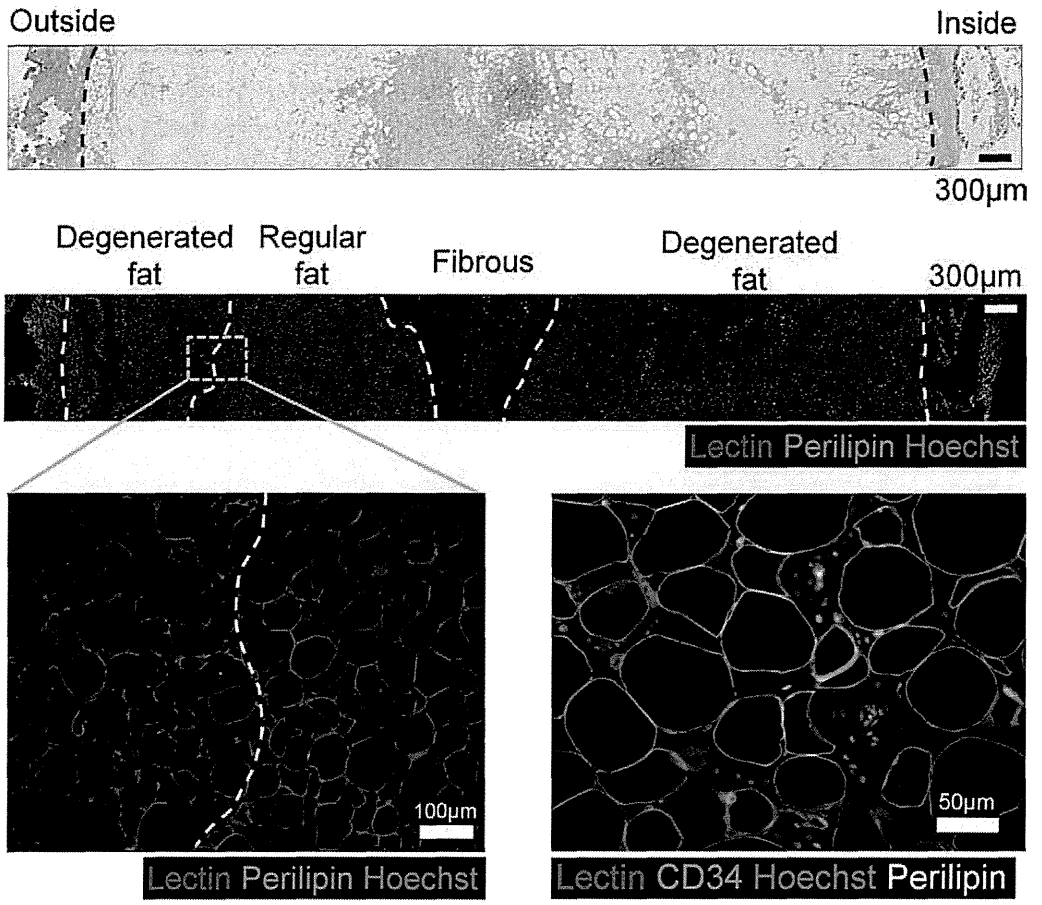

Fig. 2. Histologic analysis of the cyst wall of the patient in case 1. Fat grafting was performed 2 years earlier and multiple cysts were left in both breasts. (**See Figure, Supplemental Digital Content 1, *http://links.lww.com/PRS/A964***.) (*Above*) Hematoxylin and eosin staining showed that surfaces on both sides of the cyst wall were fibrous layers. *Scale bar* = 300 μm. (*Center*) Immunohistochemistry showed that there were regular and degenerated fatty portions between the inner and outer fibrous layers. *Scale bar* = 300 μm. (*Below, left*) The regular fatty portions had intact round adipocytes (perilipin-positive), whereas degenerated fatty layers had many dead (perilipin-weak or -negative) adipocytes and fibrous areas. *Scale bar* = 100 μm. (*Below, right*) The regular fatty portions had many vessels and capillaries (lectin-positive) and $CD34^+$ adipose stem/progenitor cells. *Scale bar* = 50 μm.

fibrous layer (Fig. 4). Calcifications were also seen in the intermediate fibrous region of the cyst wall in cases 2 and 3 (Fig. 4, *center* and *below*) and case 3 showed most intense calcified deposits among the three cases, suggesting that calcifications may develop progressively in the cyst wall over time (Fig. 4, *below*). (**See Figure, Supplemental Digital Content 3**, *E, http://links.lww.com/PRS/A966.*)

Clinical Findings on Computed Tomography or Mammography of Long-Term Follow-Up Cases

We examined sequential follow-up computed tomographic and mammographic images in patients with oil cysts. On computed tomographic images, the cyst content was heterogeneous and the cyst wall was thick enough to be clearly detectable. The cyst had already formed at 6 months but did not change in size between 3 and 8 years, suggesting that the cyst size was final and would not change in the future (Fig. 5). [**See Figure, Supplemental Digital Content 4**, which shows sequential computed tomographic images and mammography of oil cysts, ***http://links.lww.com/PRS/A967***. Computed tomographic images were sequentially taken from a patient (34-year-old woman) with multiple oil cysts in both breasts who did not undergo any removal of the cysts. The size of oil cyst did not change between 3 and 8 years, but calcifications progressed during the period.] Calcifications in the cyst wall were not clear at 6 months, but developed gradually over time.

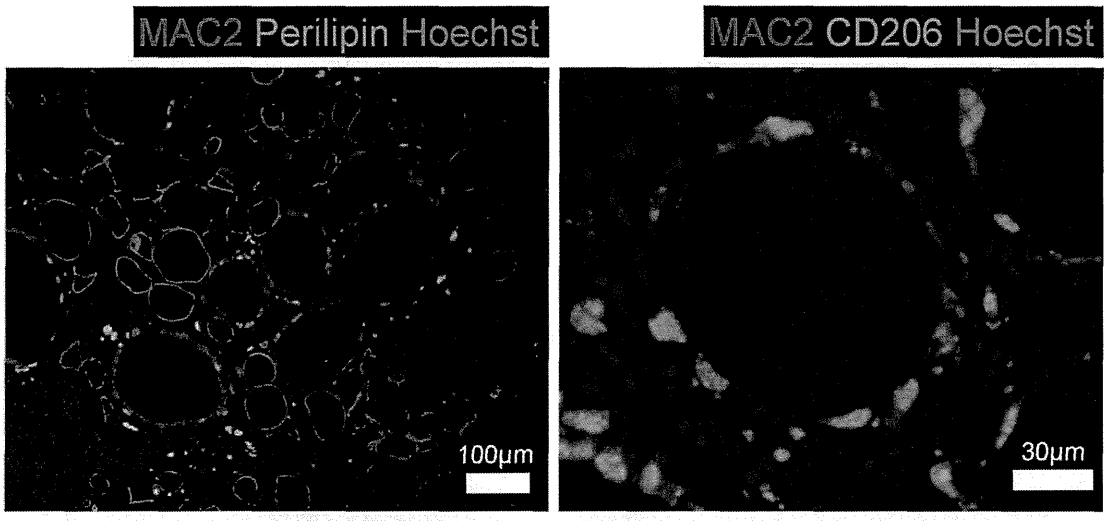

Fig. 3. M2 macrophages in degenerated portions of the cyst wall (case 2). (*Left*) Degenerated portions showed many small and large oil droplets (perilipin-negative) in the fibrous area. All oil droplets were surrounded by MAC2$^+$ macrophages. *Scale bar* = 100 μm. (*Right*) Most of the macrophages were positive for both MAC2 and CD206, indicating that they were anti-inflammatory M2 macrophages. *Scale bar* = 30 μm. (**See Figure, Supplemental Digital Content 2, *http://links.lww.com/PRS/A965*.**)

Sequential mammographic images indicated that sand-like (or small stone-like) macrocalcifications progressed over time up to several years even when no calcifications were detected at 1 year (Fig. 6). [**See Figure, Supplemental Digital Content 5**, which shows sequential mammographic images of a patient with fat grafting to the breast, ***http://links.lww.com/PRS/A968***. Mammograms were taken sequentially from a patient (30-year-old woman) who underwent fat grafting to the breast with no postoperative lumps. Calcification was not apparent at 1 year, but sand-like macrocalcifications were clearly detected at 2 years and progressed over time, indicating that calcifications grow progressively at least up to several years even with no noticeable lump. It is suspected that small necrotic areas become sand-like calcifications, whereas larger necrotic areas become oil cysts with eggshell-like calcification.] It is suspected that small areas of necrosis become sand-like calcifications, whereas large areas of necrosis becomes oil cysts with eggshell-like calcifications. (**See Figure, Supplemental Digital Content 4**, which shows sequential computed tomographic images and mammography of oil cysts, ***http://links.lww.com/PRS/A967***. Mammography of the patient at 8 years. Many eggshell-like calcifications are shown.)

DISCUSSION

Autologous fat injection to the breast has become more popular, not only for breast reconstruction, but also for cosmetic augmentation worldwide. However, it must be kept in mind how serious oil cysts are for patients and how important it is to prevent fat necrosis. As shown in this study, oil cysts are the worst outcome of fat grafting—much worse than no retention. Oil cysts show long-term inflammation and progressive calcification and problematic clinical symptoms. Indeed, they are permanently problematic; they become neither silent nor reduced in size.

Our results showed that cyst walls chronically contained degenerated fatty portions with numerous inflammatory cells, mainly M2 macrophages. The long-term existence of a degenerative fat portion indicates that the microenvironment in the cyst wall, such as oxygen tension and/or progenitor cell number, is insufficient for normal adipogenesis. Thus, chronic inflammation persists in oil cyst walls even after several years, which is presumably associated with the progressive fibrosis and calcification and the problematic clinical symptoms.

Anti-inflammatory M2 macrophages are distinguished from inflammatory M1 macrophage populations by several markers, including the interleukin-4R, mannose receptor (CD206), Arg1, and Fizzl.[19,20] Although M1 macrophages play dominant roles in phagocytosis in acute tissue remodeling, the proportion of M1 to M2 macrophages changes with the adaptive immune response from acute to chronic inflammation.[17] Monocytes attracted to a site of inflammation